PAPER F

AN APPROACH TO INTERVAL VELOCITY ANALYSIS FOR CROSSWELL REFLECTION IMAGING USING REFLECTION TRAVELTIMES

Mark Van Schaack and Spyros Lazaratos

ABSTRACT

Crosswell reflection imaging techniques require an accurate velocity model to effectively image the data. Using the VSP-CDP mapping technique, inaccuracies in the velocity model result in lateral and vertical mispositioning of reflection events. These misalignments can produce destructive interference when stacking and result in a loss of resolution. The relative mispositioning of reflection events, which degrade the stacked image, can be used to calculate perturbations to the original velocity model. In this paper we propose an approach to crosswell reflection interval velocity analysis which integrates reflection imaging and traveltime tomography. This approach reduces the labor and interpretation required by the current approach of residual static corrections and ensures the consistency of the reflection and velocity images.

INTRODUCTION

Crosswell seismic reflection imaging has recently been shown to be an effective tool for evaluating geologic structure in a region between two wells in a West Texas carbonate environment with a resolution approaching a few feet (Lazaratos, 1993). The West Texas field study yielded p and s-wave reflection images that clearly show both continuous lateral structure in a reservoir region and an angular unconformity defining the nature of a contact between formations at the base of the survey. Our interpretation of these features is supported by local geologic knowledge and by the tie with synthetic reflection images created using sonic well logs acquired in the two boreholes. Lower resolution, but important velocity information, calculated through the inversion of crosswell traveltime data,

supports and augments our interpretation of the interwell region. As with the reflection images, the tomographic image is consistent with a priori well log and geologic information.

The important next steps in making crosswell seismology useful for solving oilfield production and exploration problems include increasing interwell survey distances, making the imaging algorithms more general to handle complicated structures and acquisition geometries, and developing an integrated approach to processing the traveltime and reflection data acquired in a crosswell survey. We believe the integration of traveltime and reflection processing schemes is the most pressing problem facing crosswell imaging. This problem has a close parallel in surface seismic imaging — velocity analysis. Similar to surface seismic processing, crosswell reflection imaging requires an accurate velocity model to correctly map and stack the interwell reflections.

In this paper we review the VSP-CDP crosswell reflection imaging algorithm, show how incorrect mapping velocities lead to errors in the reflection image, and illustrate how we might use these errors as input to improve our velocity model. The crosswell seismic velocity analysis procedure we describe combines the philosophies of surface seismic velocity analysis and crosswell reflection traveltime tomography. We believe this approach to crosswell imaging will reduce the labor involved in processing crosswell data while ensuring the reflection and velocity images are consistent with one another.

VSP-CDP CROSSWELL REFLECTION IMAGING

Presently, the most effective techniques for crosswell reflection imaging are based on the VSP-CDP (Vertical Seismic Profile to Common Depth Point) mapping algorithm (Wyatt and Wyatt, 1981). This algorithm has been used in several real-data crosswell studies (Baker and Harris, 1984; Delvaux et al., 1987; Abdalla et al., 1990; Lazaratos et al., 1991). The VSP-CDP mapping technique is well suited to real-data problems because noise in the data is not smeared throughout the image. The VSP-CDP technique is best characterized as a point to point transformation and more closely resembles a sorting operation than a wavefield operator. This makes the mapping exactly invertible.

Until recently, crosswell reflection images were created using a methodology similar to that used in single offset VSP processing. Lazaratos (1993) showed the importance of multiple fold imaging in reducing ambiguities and noise. Multiple fold imaging results in a more reliable image of the interwell area than is available from any single mapped gather. Under optimal mapping conditions, the reflections will be stationary within the image while other unwanted coherent and incoherent energy moves about from gather to gather. This

effect allows stacking to remove the non-stationary noise and results in a reflection image with improved signal to noise.

The Imaging Sequence

The method developed by Lazaratos (1993) to image crosswell reflections involves several steps:

1) Mapping
2) Residual moveout corrections
3) Stacking

Prior to these three steps, the crosswell data are processed to enhance the reflected events and to minimize other unwanted energy. Rector et al. (1992) found multiple domain filtering to be effective for wavefield separation. A great deal more research is needed in the area of wavefield processing though. In particular, amplitude corrections must be developed to compensate for the effects of geometrical spreading, source and receiver directivity and coupling if seismic inversions are to be attempted. Since our primary goal for reflection imaging is, at, present to obtain information on geologic structure, or texture, many of the amplitude corrections can be applied less rigorously than would be required if the reflection amplitudes were to be analyzed in a quantitative fashion.

The processed dataset with enhanced reflections is mapped using the VSP-CDP technique. Our current implementation of this algorithm makes several assumptions including straight wells, flat reflectors, and a 1-D velocity model. Typically, the mapping velocities are determined empirically, or using a 1-D traveltime tomography inversion. Common shot gathers (CSG's) and common receiver gathers (CRG's) containing either upgoing or downgoing reflected events are mapped separately. Following mapping, four sets of mapped images exist of the surveyed zone; upgoing CRG's, downgoing CRG's, upgoing CSG's and downgoing CSG's .

One useful sort domain for processing the data at this point is the common angle gather (CAG). Data is transformed into this domain based on the angle of incidence of assumed reflections. Lazaratos (1993) used a straight ray assumption for sorting in the processing of the West Texas dataset. Reflection characteristics in a CAG are relatively stable since many of the factors that result in a change in character of the reflected wavelet are relatively constant for a given angle of incidence. Some of the factors whose effects are minimized for a constant angle of incidence are path length, AVO (amplitude versus offset), source radiation pattern, and receiver antenna pattern. Also, the moveout of reflections versus angle of incidence is minimal compared to many other coherent noise events. This

makes the CAG ideal for reflection identification. Mapped CRG's and CSG's are typically transformed into the CAG domain and combined to yield upgoing and downgoing well to well images for varying angles of incidence. Stacking these gathers at this point results in a brute stack.

Reflections can often be seen prior to stacking in the mapped gathers. In real data studies there often exist slight misalignments between reflections at a single lateral position over a range of angles of incidence. Figure 1, an example from the West Texas dataset, illustrates reflection events varying in depth over a range of incidence angles in an amplitude versus angle (AVA) gather. The AVA gather shows reflections for a constant interwell lateral point over a range of incidence angles. Stacking the crosswell data consists of stacking the traces in the AVA gather to provide a single output trace which images the reflection events at one lateral offset. The misalignments, illustrated in figure 1, are large enough that direct stacking results in a degradation in reflector quality instead of an enhancement. There are a number of possible explanations for how this might occur;

1) the assumptions of flat reflectors and vertical wells used by the mapping routine may not be valid
2) a 1-D velocity model may not be satisfactory
3) the velocity model may not have the necessary accuracy
   (even if the 1-D assumption holds).
4) velocity anisotropy
5) there may be depth errors in the source and/or receiver positions
6) there may be timing errors

Since all these potential errors could not be adequately explored and corrected for in the processing of the West Texas dataset, and the variation in reflector depths was generally less than a wavelength, the reflections were aligned prior to stacking using residual moveout corrections.

The technique for applying residual moveout corrections requires, first, an accurate reference model to measure the trace to trace static errors. Lazaratos (1993) used a spatially bandpass filtered brute stack as his reference. Reflector horizons are picked in the CAG domain over the desired range of incidence angles in the unstacked data and the reference stack. A residual correction is then calculated based on the difference in horizon depths and applied to the data in common angle gathers. Following residual moveout corrections the data are ready for stacking. Upgoing and downgoing CAG's are stacked separately. These separate stacks can be merged by reversing the phase of one stacked image before adding them together. This phase reversal corrects for the difference in sign of the reflection coefficient seen by the upgoing and downgoing energy.

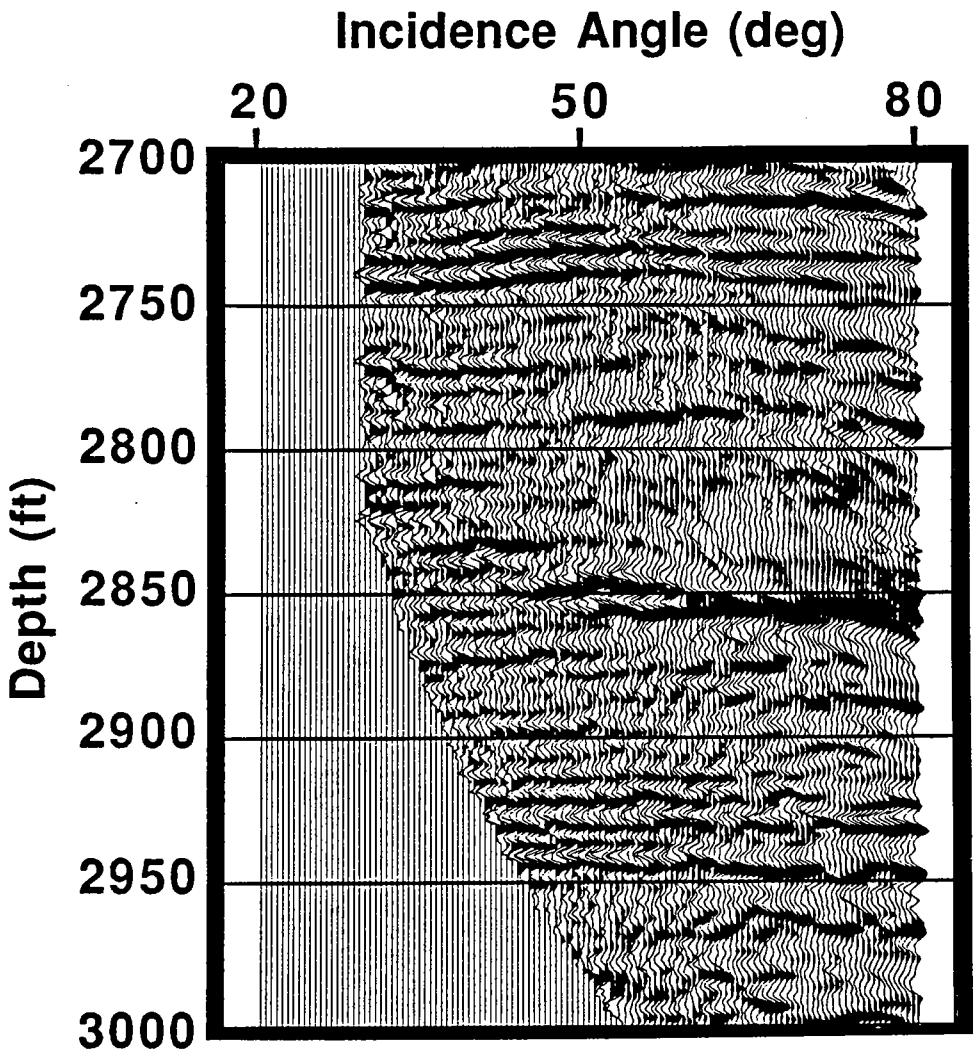

Figure 1: Amplitude versus angle gather from the West Texas dataset for p-wave downgoing reflections. The lateral interwell position of this gather is approximately 10.0 feet from the source well. Note the small shifts in the reflector depths versus angle of incidence. In particular, the reflection at approximately 2740.0 feet bows up through an angle of incidence of about 50 degrees. These misalignments will result in a loss of resolution through destructive interference when the gather is stacked.

SPATIAL MISPOSITIONING OF REFLECTIONS: THE EFFECT OF MAPPING VELOCITIES

The described reflection mapping technique depends on a velocity model accurate enough that reflections map within approximately a half wavelength of their true position. This is required to avoid gross depth errors and reflector misidentification while correcting for residual moveouts. Fortunately for work done to date with the West Texas dataset, the assumption that the velocity structure is 1-D was essentially correct. Most important was the success in imaging the velocity structure using traveltime tomography with the accuracy necessary for effective reflection processing.

Unfortunately, the ability of crosswell tomography to image the interwell velocity structure usually suffers with increasing interwell distance. This degradation in imaging ability is due in part to a reduction in angular coverage. It is often impossible to scale all aspects of geometrical coverage for crosswell surveys as well offsets increase. One difficulty faced in preserving the angular coverage may be source and/or receiver placements that are deeper than the well depths or above ground. Also, the increase in data volume and acquisition time may not be logistically realistic. It will be shown in this section, using work done by Lazaratos (1993), that for increasing well offsets, where the accuracy of traveltime tomography typically begins to decrease, the accuracy of the velocity model used in the reflection mapping must increase to preserve the coherency of the stacked reflections. This suggests that velocity estimation is indeed a fundamental issue facing the use of crosswell reflection imaging at increasing well offsets.

How Velocities Are Used In Reflection Mapping

To illustrate the importance of the mapping velocities and their effect on crosswell reflection imaging it is helpful to understand some basics of the VSP-CDP mapping technique. Figure 2 illustrates the philosophy behind VSP-CDP mapping. For this example a constant velocity medium and horizontal reflectors are assumed. For any source and receiver combination, the location of a single reflection point can be calculated for each depth. Examples of these discrete reflection points are shown by **A**, **B**, and **C**. These reflection points correspond to reflectors at depths $\mathbf{Z_a}$, $\mathbf{Z_b}$, and $\mathbf{Z_c}$. By calculating the reflection points at finer and finer depth increments we define the **mapping trajectory**.

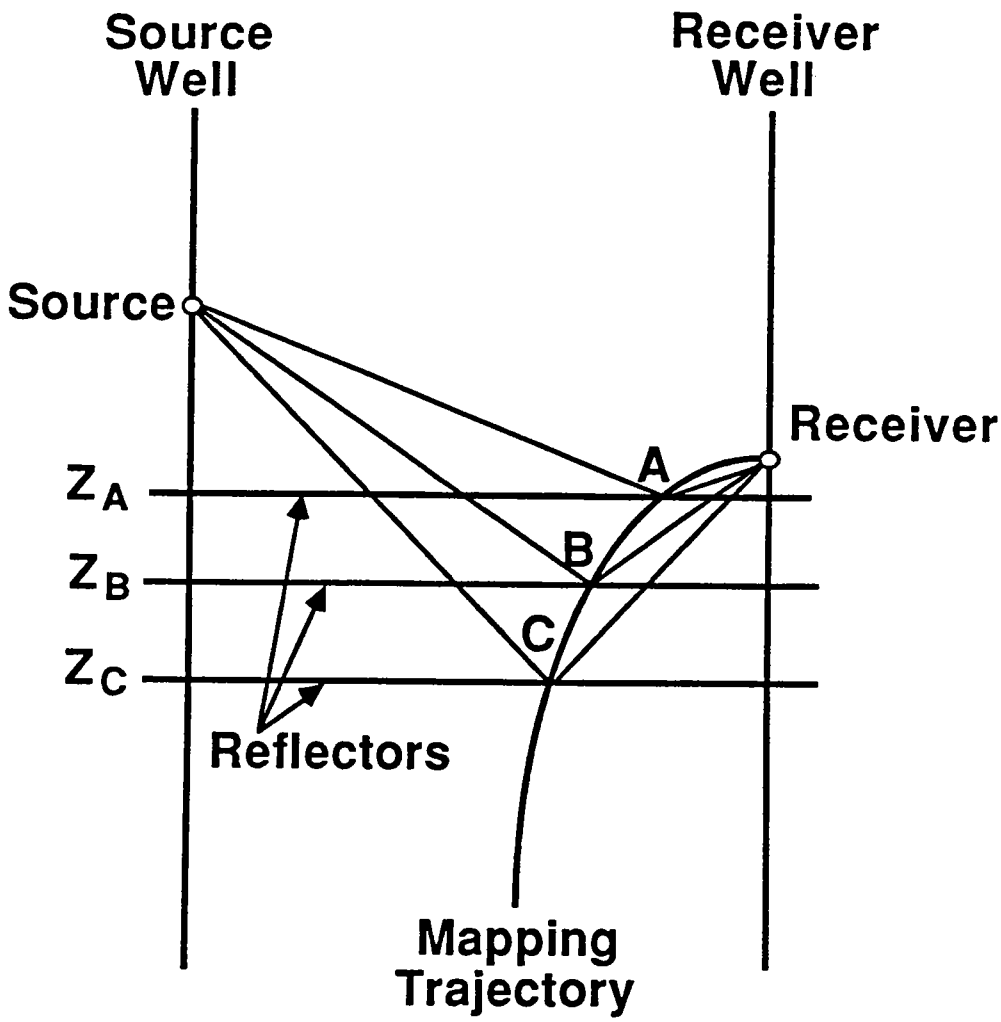

Figure 2: The VSP-CDP transform. Mapping trajectories are defined for each source-receiver pair based on the source and receiver positions, mapping velocities and reflector orientation.

Since there exists a recorded trace for each source and receiver combination, the mapping routine basically works to spread that trace along the mapping trajectory defined by the source-receiver pair. To map the trace data, the data value is positioned on the mapping trajectory so that its time and the traveltime of a raypath reflecting at that point are the same. Each point on the trace is mapped to a unique position on the mapping trajectory this way.

For a constant velocity medium and flat reflectors, the mapping trajectory is defined solely by the source and receiver locations. A velocity estimate of the medium is used to calculate the total traveltime corresponding to each reflecting raypath. An incorrect velocity model will result in mapping events incorrectly in space. Figure 3 shows how reflection points will be mispositioned due to an incorrect mapping velocity. As mentioned before, reflection mapping is basically a problem of finding the point on the mapping trajectory, corresponding to a raypath from source to receiver through that reflecting point, which has the same time as the point on the trace to be mapped. In figure 3, the traveltime of raypath **S-A-R,** calculated using the correct velocity model, equals the time of the amplitude of the trace mapped at point **A**. If the mapping velocity is too high, the raypath length must be increased to give the same traveltime. Raypath **S-B-R** shows how the path must be changed to increase the traveltime while keeping the reflection point on the mapping trajectory. In this case the data will be mapped deeper at point **B**. Notice that the data is mapped with both a vertical and lateral error in position. Also we can see in figure 3 that an incorrect mapping velocity results in an error in the measured angle of incidence, Φ. In this figure, $\Phi_{\mathbf{err}}$ illustrates the incorrect angle of incidence which results when the data are mapped using an incorrect velocity model.

The error in calculating Φ has secondary effects one of which affects how accurately the data can be sorted into different domains. One gather affected directly by this error is the CAG. As mentioned previously, the CAG is used in calculating and applying residual statics. Data is sorted into this domain using the calculated incidence angle, $\Phi_{\mathbf{err}}$, so the accuracy of the CAG suffers directly with increasing velocity errors.

The Effect of Velocity Errors in the Common Angle Gather Domain

We have shown an example of how an incorrect mapping velocity can act to misposition reflections present in a single trace. Now we address the question of how this mispositioning acts to affect the data in the CAG domain. Lazaratos derived several simple expressions in his thesis to describe the mispositioning of reflected events for the simple

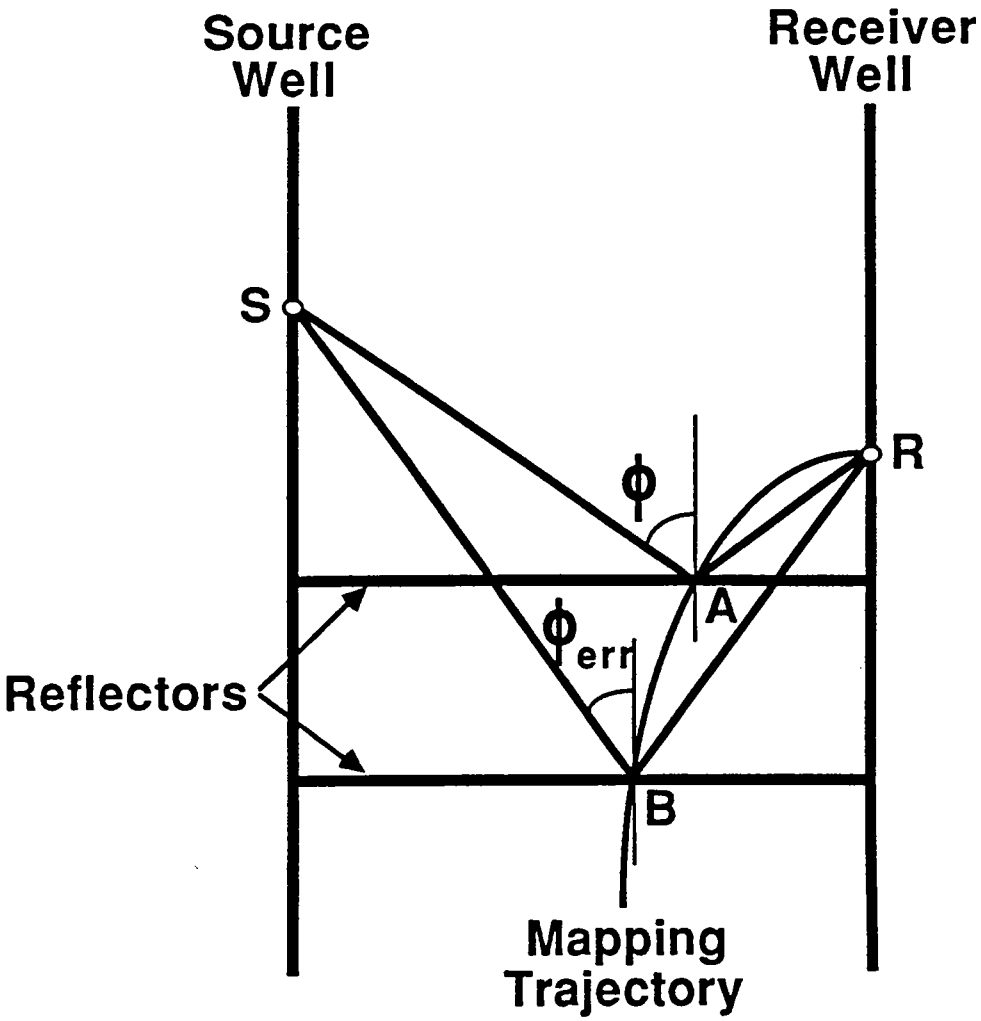

Figure 3: Mispositioning of the reflection point due to incorrect mapping velocities. In this example, correctly mapped point A is mapped at point B due to an overestimate of the mapping velocities. The traveltime of raypath S-A-R, mapped with the correct velocity, is the same as raypath S-B-R, mapped with too high a velocity. Note the error in determining Φ due to the mispositioning of the reflection point..

case of a homogeneous velocity model and horizontal reflections. We will review this work using Figure 3 to illustrate the expressions.

In figure 3 the correctly positioned event is represented by point **A**. This point is correctly mapped using the mapping velocity **v**. The angle of incidence of the ray at the reflection point is denoted by Φ. Perturbing the mapping velocity by Δv results in the data being mapped incorrectly at point **B**. The vertical mispositioning is represented by Δz and the lateral mispositioning by Δx. Using this nomenclature, Lazaratos' expressions can be stated as follows:

$$\frac{\Delta x}{x_{well}} = \frac{1}{2}\left[2\left(\frac{x}{x_{well}}\right) - 1\right]\left(1 - \frac{1}{\sqrt{1 + \frac{\left(\frac{\Delta v}{v}\right)^2 + 2\left(\frac{\Delta v}{v}\right)}{\cos^2\Phi}}}\right) \qquad (1)$$

$$\frac{\Delta z}{x_{well}} = \frac{1}{2\tan\Phi}\left(1 - \sqrt{1 + \frac{\left(\frac{\Delta v}{v}\right)^2 + 2\left(\frac{\Delta v}{v}\right)}{\cos^2\Phi}}\right) \qquad (2)$$

Notice in the above equations that the error is normalized by the interwell distance. This has important ramifications for crosswell reflection imaging. Most importantly, to keep the mispositioning error the same at larger well offsets the velocity error must reduced. Also note that vertical and horizontal mispositioning for a given velocity error is a function of the angle of incidence. Plots illustrating the degree of vertical and lateral mispositioning as a function of incidence angle and velocity error are shown in figure 4.

Several different points can be noted from the plots in figure 4. First, the normalized lateral error increases monotonically for increasing angles of incidence and the mispositioning error is larger for larger velocity errors. More important is the relationship of vertical mispositioning error to angle of incidence. In this plot we can see the mispositioning error is minimized at the intermediate angles of incidence around 45-50 degrees. The vertical mispositioning increases for all degrees of velocity error away from these intermediate angles.

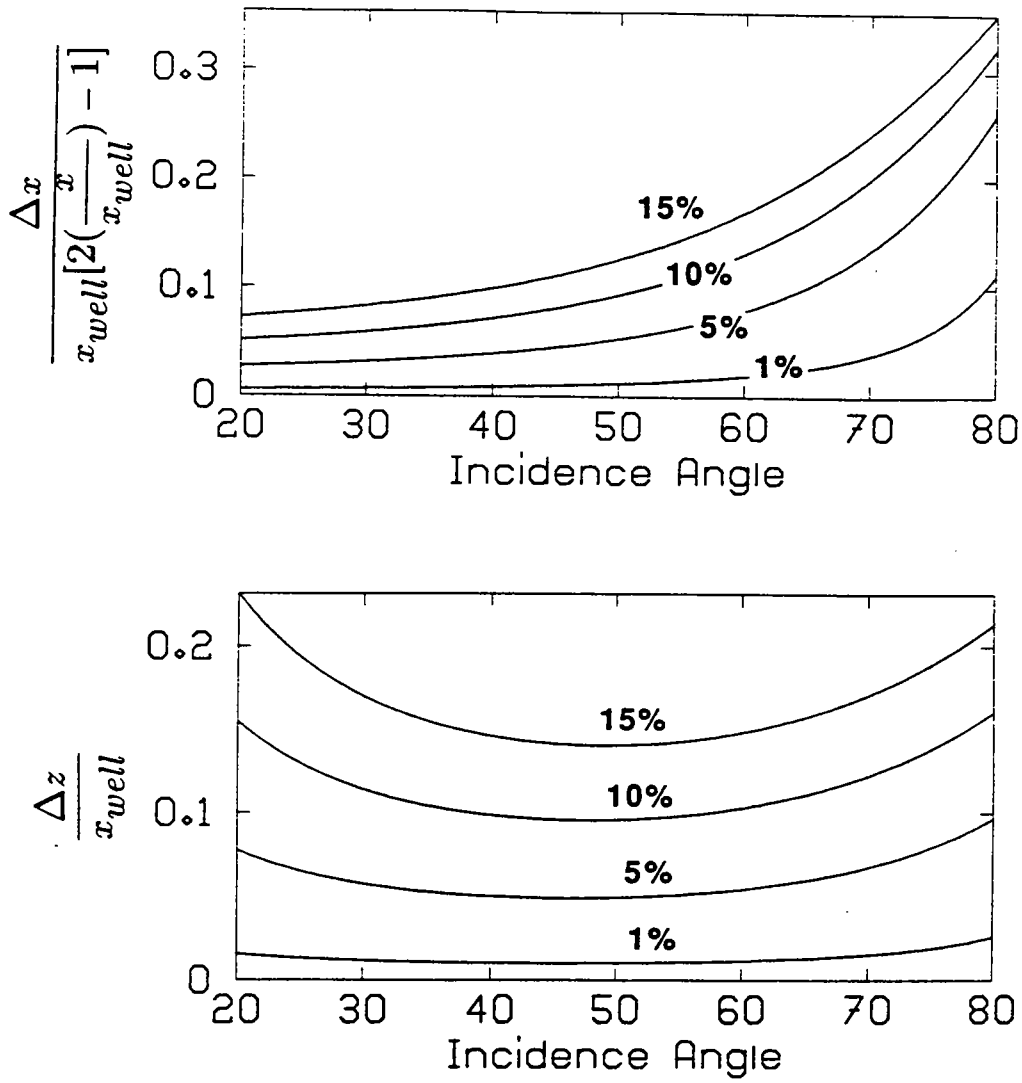

Figure 4: Lateral and vertical mapping errors for different percentage errors in the mapping velocity. The incidence angle is the true incidence angle at the reflector. Note the vertical mispositioning is at a minimum for incidence angles of approximately 45-50 degrees.

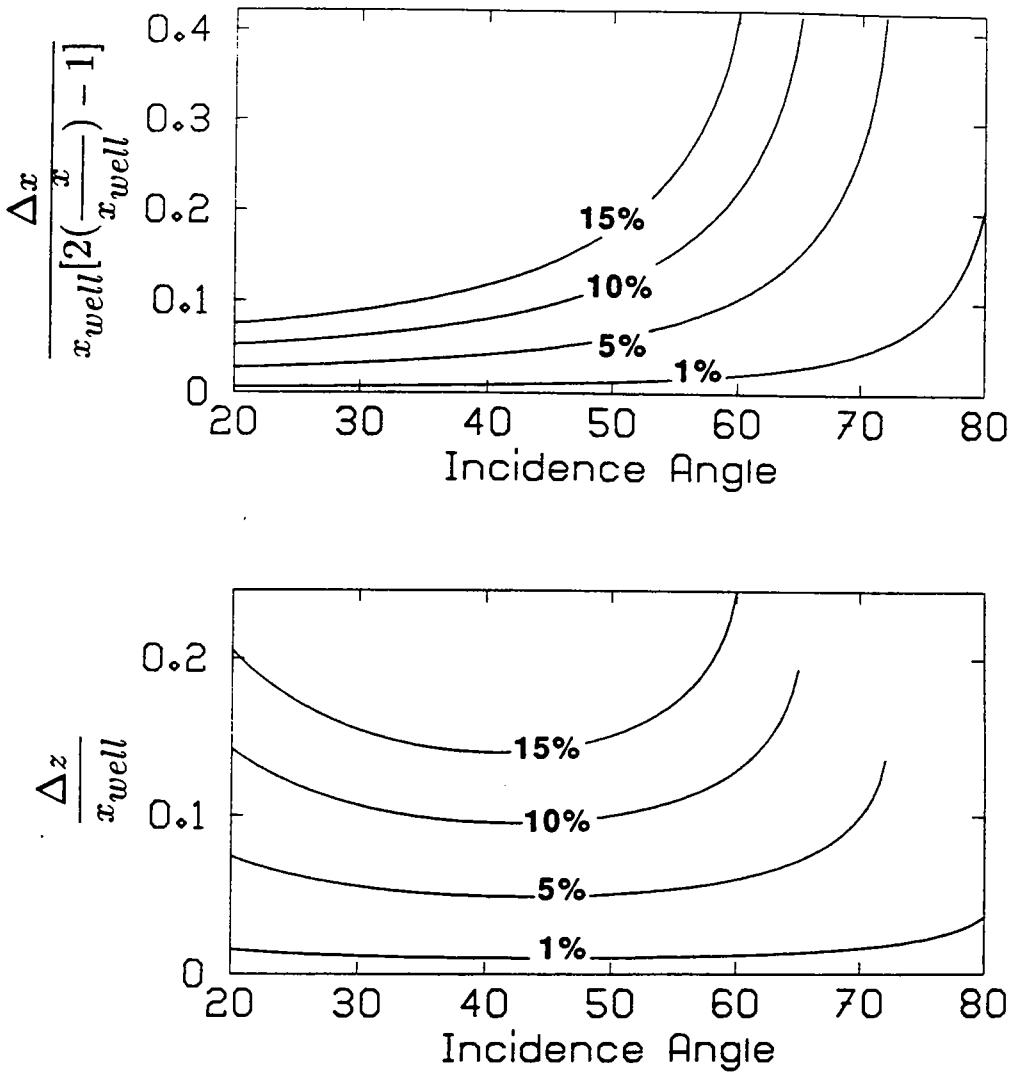

Figure 5: Lateral and vertical mapping errors for different percentage errors in the mapping velocity. The incidence angle is this diagram is Φ_{err}, (see figure 3) the erroneous incidence angle calculated using the spatially mismapped data Note that although the trends are the same as figure 4, the sensitivity of spatial mispositioning is more sensitive to incidence angle.

Figure 5 illustrates the effect of incorrect mapping velocities on reflector positioning as a function of the incorrectly calculated incidence angle, Φ_{err}. As can be seen from the plots, the trends of the vertical and lateral mispositioning errors are the same as those calculated when the positioning error is plotted against the true incidence angle Φ. The primary difference is that the magnitude of the mispositioning error increases more quickly moving away from the error minima. Since the degree of error in the mapping velocity estimate will typically be unknown, CAG sorts will actually be made with respect to Φ_{err}.

How Velocity Errors Affect the Stack

Using the CAG domain it is easy to visualize how vertical mispositioning results in a degradation in stack coherency. The final stack is created by summing the AVA gathers over the desired range of angles. If the velocity error is not small, and the range of incidence angles used is not small, the reflected events will not stack coherently. In real data situations, the largest range of incidence angles is preferable to increase the signal to noise level of the stack.

To better illustrate how reflections are mispositioned by velocity errors we performed several mapping simulations using a full waveform synthetic dataset created with Sierra Geophysics' wavefield simulation program VESPA. Figure 6 shows the basic geometry of the crosswell simulation and the model. The simulation was run with 101 shot and receivers positioned vertically every 5 feet starting at the reflector. The wavelet used is a 100-1000 Hertz zero-phase Ricker. In order to illustrate the equations shown above, the model was created using a single velocity of 10,000 feet/second. A single interface is created by a density contrast across the interface at 2000 feet. VESPA allows the separation of upgoing and downgoing wavefields in the calculation phase. This feature was used to make it possible to bypass the wavefield separation phase. Trace amplitudes were normalized by their peak value.

The full wave data were mapped using three different mapping velocities and sorted into the CAG domain for display. Figures 7-12 show the results in the CAG domain. The data are presented in wireframe plots to allow the curvature of the spatial mispositioning to be seen. In figures 9 and 10 the data are displayed having been mapped with the correct mapping velocity. Note the reflectors are flat both versus lateral point and versus incidence angle. For higher angles of incidence, the reflections reach the critical angle and the reflections change phase. Figures 7 and 8 illustrate the results of using an estimate of the velocity which is 15% low. Reflections at all angles of incidence are mapped shallow. As

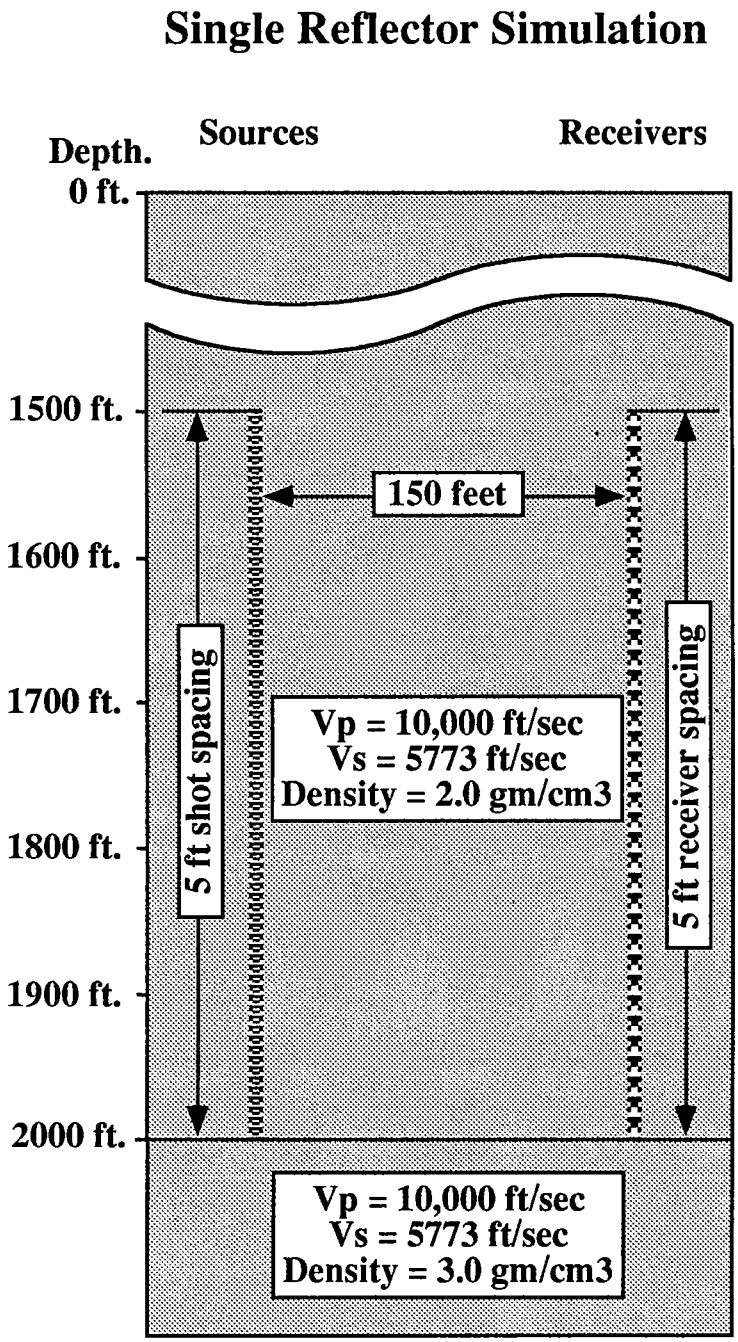

Figure 6: Model for full wave single reflector simulation. The compressional and shear velocities of both layers are equal. The reflector is defined by the density contrast.

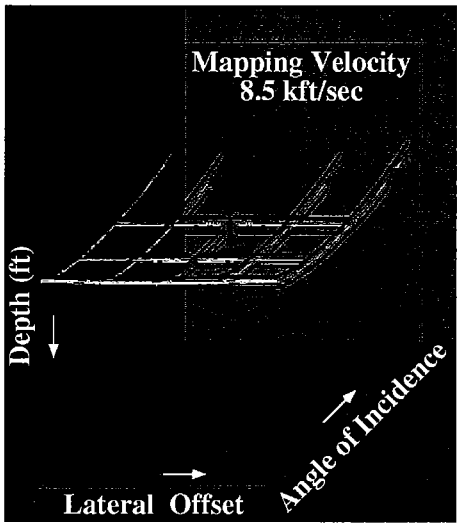

Figure 7: Reflector mapped at 8.5kft/sec. (front)

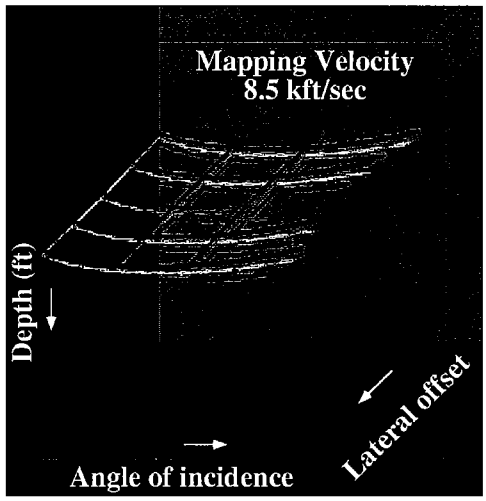

Figure 8: Reflector mapped at 8.5kft/sec. (side)

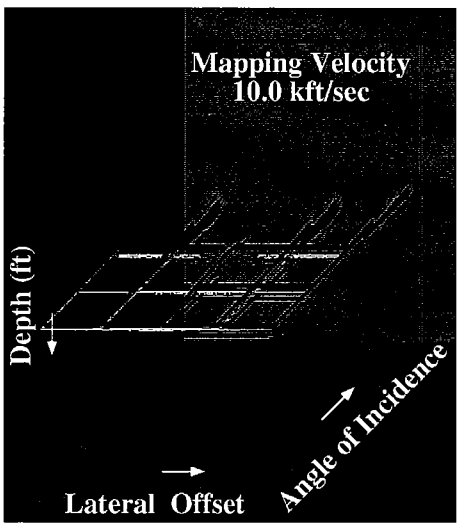

Figure 9: Reflector mapped at 10.0kft/sec. (front)

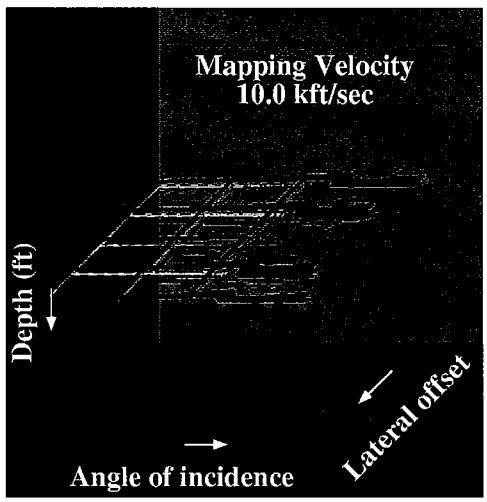

Figure 10: Reflector mapped at 10.0kft/sec. (side)

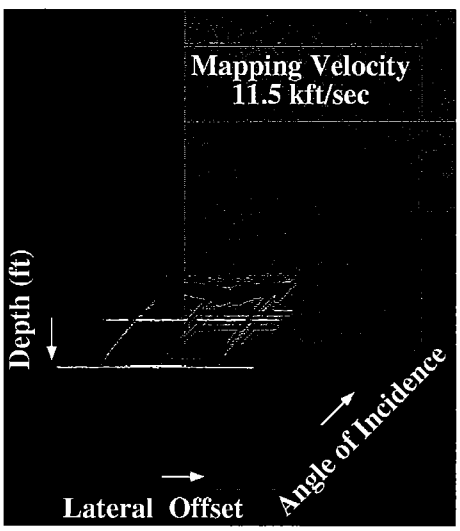

Figure 11: Reflector mapped at 11.5kft/sec. (front)

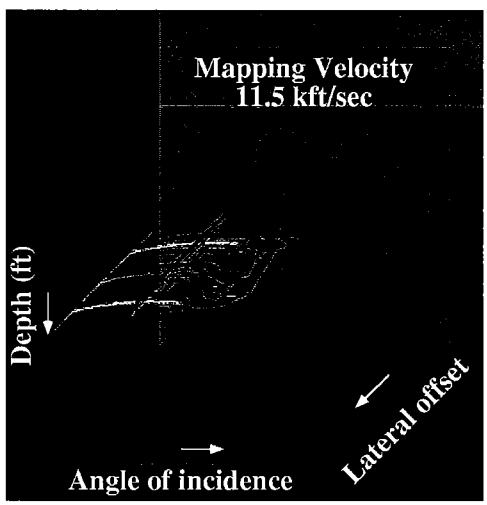

Figure 12: Reflector mapped at 11.5kft/sec. (side)

predicted by the equations, reflections at the lower and higher angles of incidence map with a larger error than those of intermediate angles of incidence. Spatial mispositioning in depth is seen to be constant for a given angle of incidence, also as predicted. Figures 11 and 12 show the results of mapping with a velocity estimate which is 15% high. As opposed to figures 7 and 8, these reflections are mapped deep. The depth errors are also a function of angle of incidence but not lateral position,

Stacking the data involves summing each AVA gather over a range of incidence angles. To obtain the highest quality stack, the reflection must be aligned properly so as to avoid destructive interference. Errors in velocity hurt the reflection image in two ways; the reflections are mapped off depth in an absolute sense, and the reflections are mapped off depth with respect to each other for varying angles of incidence. Our goal is modify the mapping velocity model to minimize these two errors.

APPROACH:
VELOCITY ANALYSIS VS. REFLECTION TRAVELTIME TOMOGRAPHY

We have shown the critical importance of an accurate velocity model to optimally map crosswell reflection data. We have also briefly discussed how interval velocity information can, by itself, be useful in estimating rock and reservoir properties. Equations have been shown relating the mispositioning of reflectors as a function of incidence angle for simple media using the domain of Common Angle Gathers. These points suggest the need and potential to develop a technique for integrating interval velocity analysis with reflection imaging. A technique such as this will result in consistent crosswell seismic imaging which will allow more reliable processing and interpretations of the crosswell data.

The technique we propose to accomplish this integrated imaging is a mixture of the philosophies of traveltime tomography and velocity analysis. Reflection traveltime tomography has yet to be successfully used in the processing of crosswell seismic data. Although including reflection data in the tomographic inversion has the advantage of increasing angular coverage, the primary stumbling block to crosswell reflection tomography has been the inability to identify and pick reflection arrival times directly from the crosswell data. Reflected arrivals are often not readily apparent among the other scattered energy in the crosswell data. This makes picking a phase event, such as a peak, extremely difficult. Also there is the additional difficulty of estimating the path taken by the reflected energy.

Reflections are often observable in the intermediate and final stages of the crosswell reflection imaging. More importantly, reflected events can be followed through a range of

incidence angles in the AVA gather. As shown previously, incorrect mapping velocities will lead to a moveout of the reflected events versus angle of incidence. The goal is to devise a processing technique to allow us to make use of the moveout of the reflected events to update the original velocity model. By minimizing the moveouts of the reflectors we achieve a better stack. Since the mapping velocities are in fact interval velocities, the optimal velocity model for reflection mapping should also be our best representation of the velocity structure since it contains all the data of the direct arrival traveltime plus data from the reflections. Including reflection data in our traveltime inversion should reduce the degree of non-uniqueness in the result. This will lead to a better reflection image and a higher resolution interval velocity tomogram.

In the sense that the data to be minimized are the reflection moveouts, this procedure is similar to surface seismic NMO velocity analysis. On the other hand, NMO velocity analysis is capable of only directly estimating stacking velocities which align reflections in time. To align the mapped crosswell data in space we must calculate a new mapping velocity model and remap the data. Although there may be a number of ways to estimate an updated velocity model based on reflection moveout, we have chosen reflection tomography as the means of inverting the reflection data technique.

Integrated Processing Technique

The processing technique we envision to refine the interval velocity model is reflection traveltime tomography. In particular, we plan to modify our current STRING tomography algorithm to incorporate reflection traveltimes. This type of inversion allows us to backproject traveltime residuals along reflected raypaths in a rather straightforward manner. With this technique we can rerun the traveltime tomography using both direct and reflected arrivals similar to the original direct arrival tomographic inversion.

Figure 13 illustrates the flow of our velocity analysis routine. As can be seen, direct arrival traveltime tomography provides the initial estimate of the velocity structure to be used for reflection mapping. Following mapping and CAG transform, the direct arrival and reflected arrival traveltime residuals are measured. If the residual falls below a user defined threshold the mapped reflection image and velocity tomograms are deemed to be consistent and satisfactory. If the residuals exceed the threshold, the data are fed into the reflection traveltime tomography algorithm. This tomographic inversion includes both the direct arrival and reflected arrival data and is run with a similar philosophy as the direct arrival only inversion. The resulting velocity model is used to remap the data and this routine is repeated until the solution criteria are met.

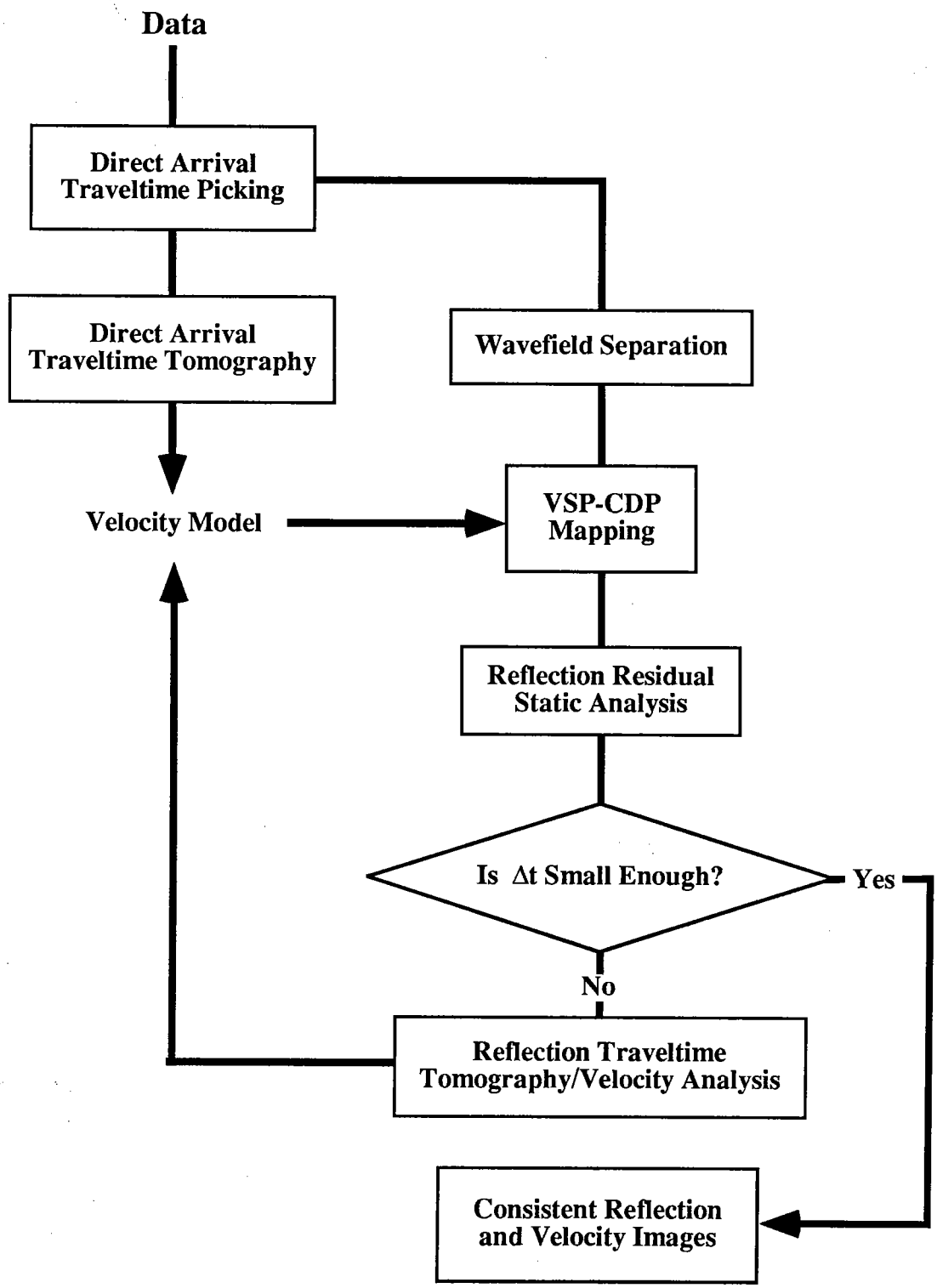

Figure 13: Schematic flow of velocity estimation processing stream.

Estimating Reflection Traveltimes And Raypaths

Reflection traveltime tomography has the same basic data requirements as direct arrival traveltime tomography; raypaths, calculated traveltimes, and measured traveltimes. In our tomographic inversions, direct arrival raypaths and calculated traveltimes are both computed using a velocity estimate and a ray-theoretic approach. Normally, direct arrival measured traveltimes are the most straightforward data to be extracted from the crosswell seismic wavefield and are picked manually. Unfortunately, as was mentioned previously in this paper, manually picking reflections in raw crosswell data is almost impossible. Even when the reflections can be seen they are typically cut up by all types of scattered energy making the normal phase picking criteria unfeasible. Also, it is difficult to establish a technique of matching calculated reflected raypaths and traveltimes to traveltime picks in the wavefield. What is required is a robust automated technique of extracting the traveltime data in a way that allows us to estimate the raypaths also. The technique we envision for extracting reflection traveltime and raypath information utilizes the VSP-CDP reflection imaging technique and the moveout of reflections for varying angles of incidence.

Our method for extracting reflection information will assume flat reflectors like the VSP-CDP mapping technique described by Lazaratos (1991), In contrast, the velocity model will be allowed to vary in two dimensions. To illustrate the technique we use the single reflector model described earlier. Figure 14 reviews how a reflector appears in a single shot gather. Each receiver location corresponds to a trace in the record. Figure 15 shows points from this reflection being mapped correctly to their true spatial positions using the correct mapping velocity. The traveltimes of the reflected raypaths equal the trace time of the reflection for each trace.

Figure 16 illustrates a situation where the mapping velocity estimate is too high. Notice first that the predicted direct arrival traveltimes plot earlier in time than the measured direct arrivals. A direct consequence of this is that the reflection will not tie at the well, and in this case will not even reach the well. Note how the reflection data is mismapped deep but still on the mapping trajectory. Also note that the error in depth changes as the reflection point moves toward the midpoint of the wells. The angle of incidence is decreasing from angles less than 45-50 degrees so the error increases. These phenomena are explained by the curves in figure 4 and by equation 2.

Figure 17 is a close-up of the spatial mismapping of the reflector. Data for reflection traveltime tomography can be extracted from this gather. Recall that the three items we require are calculated raypath, calculated traveltime, and measured traveltime. All three of these items are available through the following measurements;

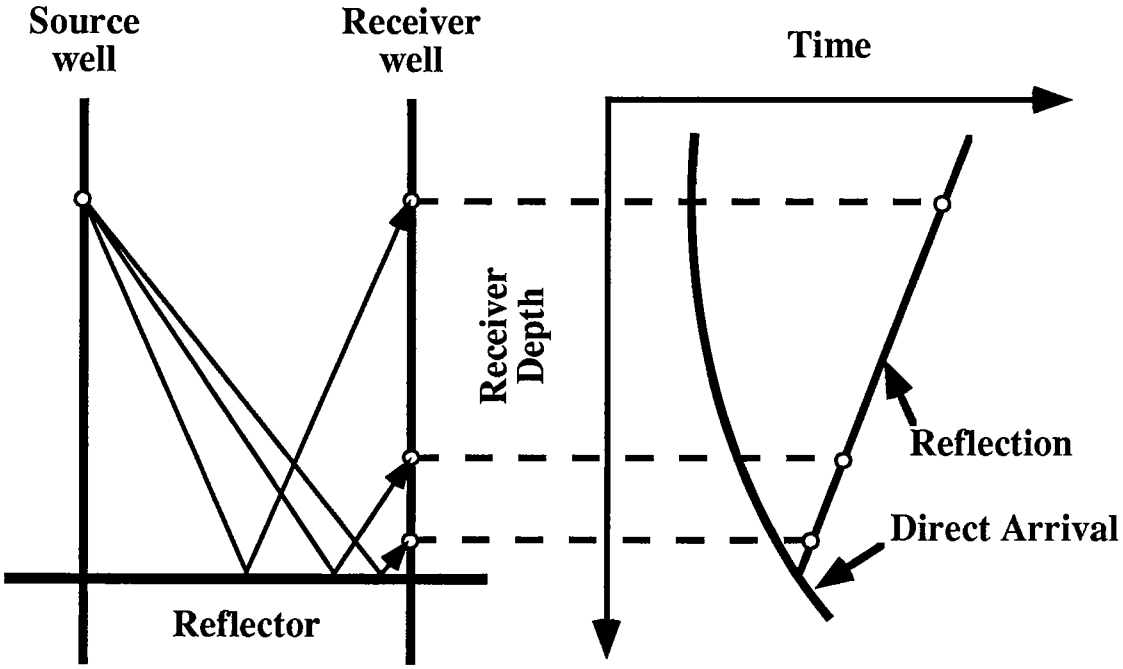

Figure 14: Data acquisition. A single reflector in a single velocity medium. At each receiver position two arrivals are measured, the direct arrival and the reflected arrival.

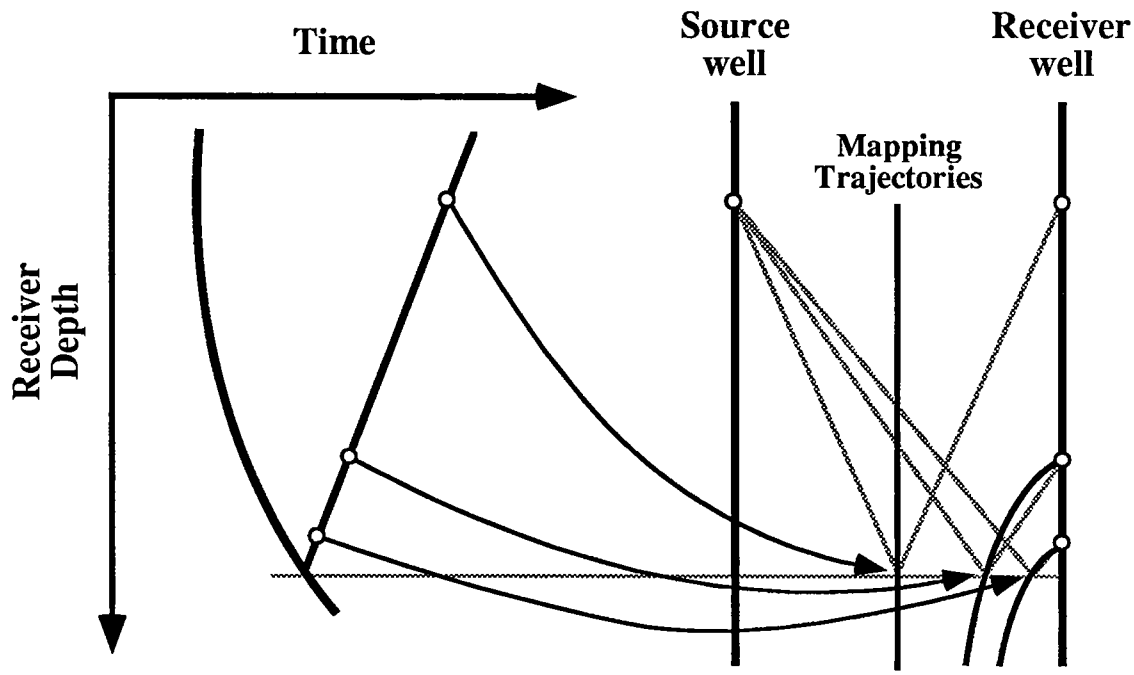

Figure 15: VSP-CDP mapping. With an assumed velocity model, mapping trajectories are calculated for each source-receiver combination. The trace corresponding to each source -receiver pair is spread along the mapping trajectory. If the velocity model is correct, as in this case, the traveltime of the raypath from source to reflection point to receiver equals the time of the reflection event in the gather and the reflection is mapped in the correct spatial position.

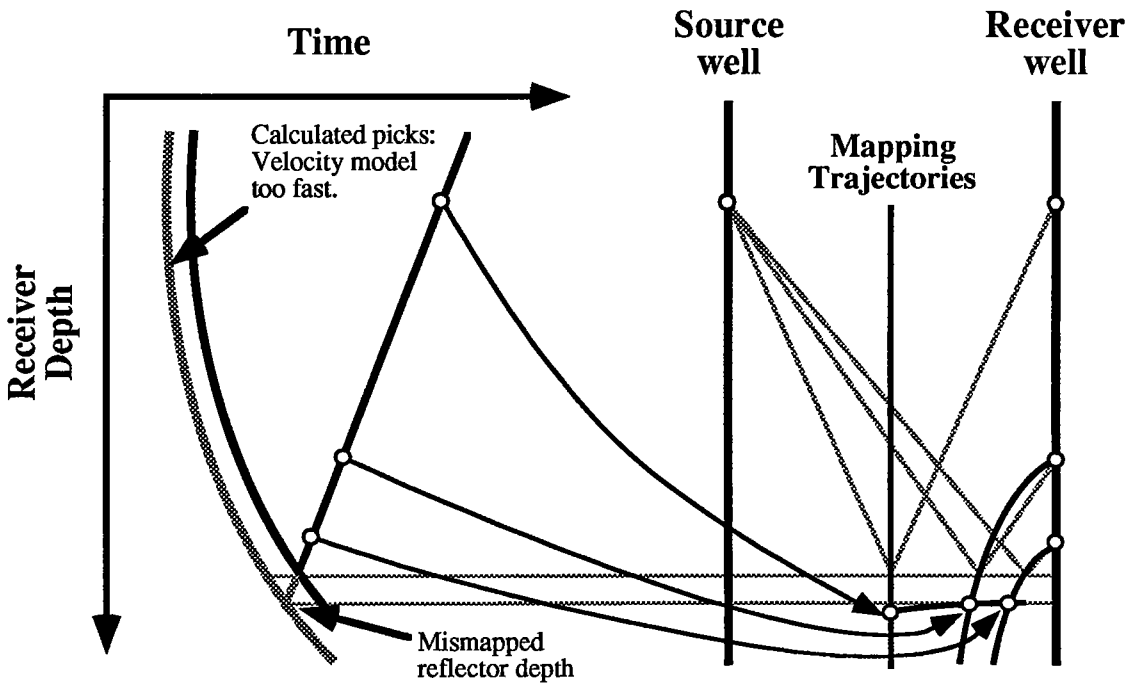

Figure 16: VSP-CDP mapping with mapping velocity too high. This figure illustrates how the reflector will be spatially mismapped when an incorrect mapping velocity is used. The reflectors are mapped deeper because the mapping compensates a higher velocity with longer raypaths to keep the traveltimes the same.

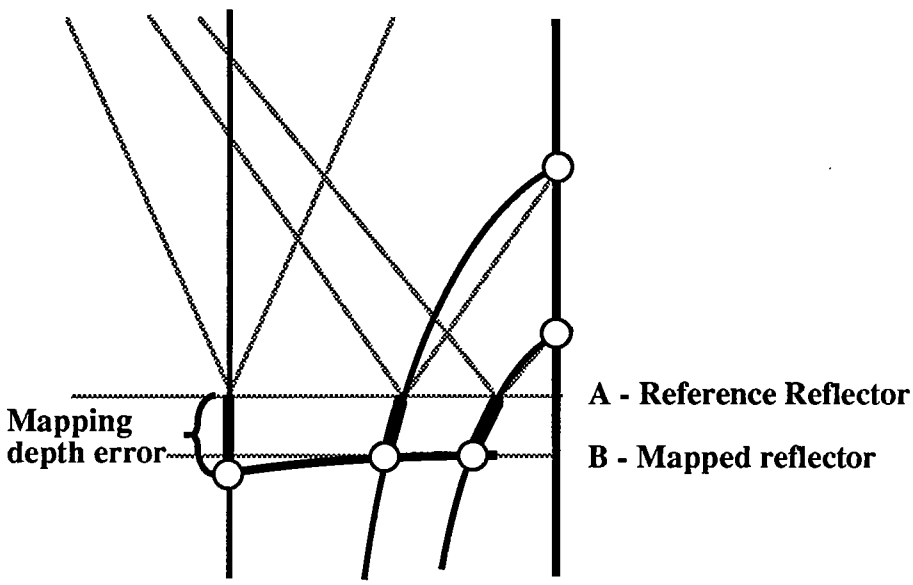

Figure 17: A closeup of the spatial mispositioning. The spatial mapping errors, the bold section of the mapping trajectories, correspond to a Δt traveltime. Reflection traveltime tomography is implemented by backprojecting this residual traveltime over the raypaths.

1) Reference reflector depth (Point A)

2) Traveltime residual (Δt)

3) Reflector mapping depth (Point B)

In the simulation, the reference reflector depth is known. Under normal conditions we will assume reflector depths at constant depth increments and extract the data each depth. The reflector mapping depth must be calculated from the relationship of the measured first breaks and the predicted first breaks. If the measured first break and the calculated first break are equal, then points A and B will be at the same depth. This does not preclude a depth shift of the reflector laterally, but we know the reflector must be mapped with no vertical error.

The gross depth error of the reflector at the well is defined by the difference in depth of points A and B. This makes the trace nearest the well the reference trace. The total error for every other trace is equal to the gross error of the reference trace plus the static shift between the two. Once the depth errors are known, they can be converted to traveltime residual errors. The residual error equals the difference in times represented by the mapping trajectory at the mapped depth and the mapping trajectory at the reference reflector depth. The calculated raypath corresponding to this residual connects the source and the receiver through the point defined by the intersection of the mapping trajectory and the reference reflector depth.

It is likely that identifying reflections in field data will be complicated due to noise levels. To handle this we anticipate using the CAG and AVA gathers to aid us in reflection identification and traveltime estimation. We know that reflectors should appear flat in this domain. Based on the reference reflector depth and the reflector mapping depth we can compute the gross depth error. By calculating the relative depth shift between the first trace and each subsequent trace using a cross-correlation or some equivalent technique, we can calculate the static shifts for all the traces. Once the total error is known for each trace, the calculation of traveltime residual and true raypath is exactly as described in the CSG case.

One advantage of this technique, which makes it practical for real data situations, is that reflections are not actually picked in the same sense as first break arrivals are picked. The exact location of the peak is not used, rather the relative depth offset between traces at approximately, the same depth is determined and then added to the gross depth error calculated using the first trace. This allows us to assume reflections at constant depth intervals over the mapped region, calculate the gross depth error based on the reflector reference depth and the reflector mapping depth, then determine the total depth offset by calculating the depth perturbations between traces. These perturbations are then used to determine the true reflection point for each raypath and the traveltime residual.

The reflection traveltime data can be easily stored in a format conducive to traveltime tomography. The mapped area is defined by reflector reference depths and binned lateral positions. These are in essence, x and z coordinates of the survey area. Following reflection traveltime analysis, each x and z coordinate represents an array of reflection traveltime data stored as raypath and residual pairs. The raypath in this format can be represented by its angle of incidence. Traveltime tomography using this data, in addition to the direct arrival data, proceeds in the same way as direct arrival only tomography. Rays are shot and residuals are backprojected over them. In this case rays are also shot from within the surveyed zone in both the forward and reverse directions to connect with the appropriate source and receivers. The traveltime residuals are backprojected along these rays in the same way as the direct rays.

CONCLUSIONS

We have outlined a proposal by which we integrate traveltime tomography and reflection imaging. Reflection traveltime and raypath data are obtained from the mapped CAG's and AVA gathers. These data are obtained through the analysis of the spatial mispositioning of reflection events which are then transformed into traveltime residuals and raypaths. This makes it possible to use both direct arrival and reflection traveltime data in a tomographic inversion. Utilizing reflection data in the traveltime tomographic inversion will improve overall angular coverage, and specifically, improvements in resolution should be realized near the top and bottom boundaries of the survey where coverage is typically very poor. Also, we are performing a velocity analysis on the reflection data in the sense that we are attempting to minimize the spatial mispositioning of the reflection images prior to stacking through the use of an improved velocity model. This type of velocity analysis should improve the overall reflection imaging procedure by aligning events and minimizing the need for residual static corrections. It also results in velocity and reflection images which are consistent. This should lead to more reliable, accurate interpretations of the interwell region.

REFERENCES

Abdalla, A. A., Stewart, R. R., and Henley, D. C., 1990, Traveltime inversion and reflection processing of cross-hole seismic data: Expanded abstracts of the 60th Ann. Internat. Mtg., Soc. Expl. Geophys., 47-50.

Baker, L. J., and Harris, J. M., 1984, Cross-borehole seismic imaging: Expanded abstracts of the 54th Ann. Internat. Mtg., Soc. Expl. Geophys., 23-25.

Delvaux, J., Noual, G., Nicoletis, L., and Dutzer, J. F., 1987, Acquisition techniques in cross-hole seismic surveys: 62nd Ann. Tech. Conf. and Exhib. of the Soc. of Pet. Eng., 413-419.

Lazaratos, S. K., Rector, J. W., Harris, J. M., and Van Schaack, M. A., 1991, High resolution imaging with crosswell reflection data: Expanded abstracts of the 61st Ann. Internat. Mtg., Soc. Expl. Geophys., 1, 150-153.

Lazaratos, S. K.,1993, Crosswell reflection imaging: Ph.D. thesis, Stanford University.

Rector, J. W., Lazaratos, S. K., Harris, J. M., and Van Schaack, M. A., 1992, Extraction of reflections from cross-well wavefields: Expanded abstracts of the 62nd Ann. Internat. Mtg., Soc. Expl. Geophys., 54-57.

Wyatt, K. D., and Wyatt, S. B., 1981, Determination of subsurface structural information using the vertical seismic profile: Expanded abstracts of the 51st Ann. Internat. Mtg., Soc. Expl. Geophys., 1915-1949.